Arabian Journal of Chemistry (2020) 13, 6682–6695

King Saud University

Arabian Journal of Chemistry

www.ksu.edu.sa
www.sciencedirect.com

ORIGINAL ARTICLE

Enhancing the performance of porous rice husk silica through branched polyethyleneimine grafting for phosphate adsorption

Nur Diyana Suzaimi [a], Pei Sean Goh [a,*], Nik Ahmad Nizam Nik Malek [b], Jun Wei Lim [c], Ahmad Fauzi Ismail [a]

[a] *Advanced Membrane Technology Research Centre (AMTEC), Universiti Teknologi Malaysia, 81310 Skudai, Johor Darul Ta'zim, Malaysia*
[b] *Department of Biosciences, Faculty of Science, Universiti Teknologi Malaysia, 81310 Skudai, Johor Darul Ta'zim, Malaysia*
[c] *Department of Fundamental and Applied Sciences, Centre for Biofuel and Biochemical Research, Institute of Self-Sustainable Building, Universiti Teknologi PETRONAS, 32610 Seri Iskandar, Perak Darul Ridzuan, Malaysia*

Received 7 March 2020; accepted 18 June 2020
Available online 25 June 2020

KEYWORDS

Phosphate;
Adsorption;
Branched polyethyleneimine;
Rice husk nano-adsorbent;
Porous silica

Abstract Removal of phosphate is necessary to prevent eutrophication and remediate other environmental issues. In this study, branched polyethyleneimine (bPEI) was grafted onto rice husk porous silica (RSi-bPEI) to enhance the selective adsorption of phosphate. The adsorption tests for phosphate were performed at various conditions to assess the effects of pH, dose, initial concentration, and contact time. As confirmed by FTIR-spectra, it was proposed that phosphate species anchored onto RSi-bPEI through ion-exchange and hydrogen bonding. The increase in positive charge of RSi-bPEI, which was due to the presence of protonated amine, played a key role in offering more adsorption sites to augment the adsorption by means of electrostatic attraction. Consequently, RSi-bPEI exhibited q_m of 123.46 mg g^{-1}, which was two-fold better than that of RSi. The adsorption behavior was best described by Langmuir isotherms and the pseudo-second-order kinetics model. Based on the competitive study, the co-existing anions did not interfere with adsorption due to the fact that phosphate could form both inner and outer sphere complexes. In addition to the high performance, high efficiency in wide pH range as well as good stability and easy recyclability are the other promising criteria of RSi-bPEI that promote its practical usage in treating phosphate-induced eutrophication of water bodies.

* Corresponding author.
E-mail address: peisean@petroleum.utm.my (P.S. Goh).
Peer review under responsibility of King Saud University.

ELSEVIER Production and hosting by Elsevier

1. Introduction

In lights of the ramification of phosphate pollution to the ecosystem, researchers have innovated many treatment methods in both laboratory and pilot scale to effectively eliminate

https://doi.org/10.1016/j.arabjc.2020.06.023
1878-5352 © 2020 Published by Elsevier B.V. on behalf of King Saud University.

the pollutants from water sources. Among the available techniques, adsorption has been lauded as an effective and versatile technique in industries for practical wastewater treatment applications (Gupta et al., 2015; Nasir et al., 2018). Adsorption of phosphate (or other pollutants) from aqueous solution is typically performed by thoroughly mixing the adsorbent with adsorbate for a desired period. Batch adsorption process is highly promising for water treatment application due to its flexibility and ease of operation.

By far, various kinds of materials have been assessed for their potential in phosphate anion adsorption. Focus has been placed on designing robust and environmentally friendly nano-adsorbent which can be obtained through simple and industrial favorable synthesis and modification processes. Local agro-wastes are alternative to the expensive precursor used for the synthesis of adsorbent. Of all the numerous adsorbents exist, porous materials have attracted considerable attention for its wide variety of applications and one of them is porous silica which characterized by good adsorption and cation exchange capability, great chemical stability and high reactivity for surface modification (Moritz and Geszke-Moritz, 2019; Omotunde et al., 2018). Interestingly, silica source can be feasibly synthesized from rice husk (RH) that is available in plentiful quantity and normally being discharged in landfills. Converting RH to useful materials is an attractive subject because it would help reducing environmental pollution and solving part of the environmental burdens i.e. problems associated with agricultural wastes and wastewater treatment (Salam et al., 2020).

The application of RH is largely depending on its physical and chemical properties like ash and silica content. Basically, RH consists mainly of cellulose (40–50%), lignin (20%), mineral ash (15%) and other minor constituents (Alexander et al., 2017). The ash is enriched with >90% silica "Production of high purity amorphous silica from rice husk," 2016. For that reason, RH is recognized as a promising source to produce nano-sized silica. Based on previously reported work, pure silica powder that has functional groups, the amorphous nature and physical structure similar to that of commercial silica could be extracted from RH through proper planning of pre-treatment and synthesis process (Lee et al., 2017; Patil et al., 2014; Suzaimi et al., 2019). It has been observed that chemical treatment using strong acids such as HCl and H_2SO_4 could effectively increase SiO_2 contents from 90% to >95% (Matori et al., 2009; Patil et al., 2014; Zulfiqar et al., 2015). The potential of nano-absorbents derived from RH for the removal of inorganic and organic contaminants has been explored. For instance, Chowdhury (2017) and Barbosa et al. (2018) achieved high removal of organic pollutant (dye) using RH and the composite of RH and metakaolin. In addition, several attempts have also been made to remove heavy metals using absorbents derived from RH. Hubadillah et al. (2017) efficiently separated Ni(II), Pb(II) and Zn(II) with separation efficiency up to 99% under environmentally relevant conditions using RHA - ceramic hollow fibre membrane. In other study, raw RH as adsorbent indicated significant sorption of heavy metals in the order of Pb > Cd > Cu > Zn (Alexander et al., 2017). In gas separation, the conversion of RH to activated carbon yielded a satisfying CO_2 removal from flue gas and good reusable capacity up to twelve cycles (Yaumi et al., 2018).

Despite the abovementioned efforts, the application of porous silica derived from RH to remove inorganic pollutants such as phosphate ions has been graced with little attention. Some earlier work observed that porous silica did not possess sufficient active sites to render high anion adsorption (Choi et al., 2011; Hamoudi et al., 2007; Hamoudi and Belkacemi, 2013). The negatively charged surface of SiO_2 due to the presence of Si—OH groups further impede the adsorption of anions. To address these limitations, surface functionalization or modification has been pursued to introduce functional groups that can potentially change the chemical and physical properties of silica nanoparticles. The modifications of porous silica derived from RH include the impregnation of metal/metal oxides into commercial silica (MCM-41) (Delaney et al., 2011; Huang et al., 2015), functionalization with amino groups (Ebrahimi-Gatkash et al., 2015) and preparation of silica nanocomposite (Dinker et al., 2017). The existing modification approaches are interesting but most of them are complicated, time-consuming, and not friendly to the environment (Delaney et al., 2011; He et al., 2018). Suitable and ideal adsorbent should not only possess a good removal capacity, it should also be stable, well dispersed in water, easily separated and can be efficiently regenerated. Currently, little attention has been placed on the preparation of hyperbranched polymer-containing porous silica derived from RH for phosphate ion removal. Prior studies have demonstrated that modifiying adsorbent matrix with polymer could significantly enhance the physiochemical properties especially for adsorption applications (Abukhadra et al., 2019). It was expected that the porous silica modified with hyperbranched polymer could render enhanced phosphate batch adsorption capacity, but the overall phosphate adsorption process and the mechanisms involved still deserve further exploration.

In this work, the adsorbent was developed by using RH as precursor to produce porous rice husk silica (RSi). Porosity of adsorbent is beneficial for facile mass transfer of pollutant within the pores, such as faster kinetics for the pollutant removal (Kiran and Prasad, 2019). To boost the adsorbent efficiency, the surface chemistry of RSi was substantially modified by functionalizing branched polyethyleneimine (bPEI) on RSi. The bPEI is an attractive cationic polymer with high content of primary, secondary and tertiary amine groups (Sanz et al., 2010; Thakur et al., 2017) wherein their protonation states allow them to adsorb the negatively charged ions through electrostatic interaction, ion exchange as well as hydrogen bonding (Suzaimi et al., 2019). It was expected that the modification of RSi as nano-adsorbent with the bPEI could grant high adsorptive removal of phosphate ions in aqueous medium with promising regeneration and reusability. Besides determining performance of the adsorbents via adsorption studies, the phosphate adsorption mechanism was also proposed based on the isotherm and kinetics studies.

2. Experimental

2.1. Materials

The RH (obtained from a Production Rice Mill Muar, Johor) was burnt to produce rice husk ash (RHA) and after that, sodium silicate solution. Sodium hydroxide (NaOH), hydrochloric acid (HCl 37%), cationic surfactant hexadecyl trimethyl ammonium bromide (HDTMA), methanol (CH_3-OH), and branched polyethyleneimine (bPEI) were purchased

from Sigma-Aldrich Company. Glutaric dialdehyde solution (25 wt%) potassium hydrogen phosphate (K_2HPO_4) as well as salts for the competing ions e.g. Na_2SO_4, NaCl, and $NaHCO_3$ (K_2HPO_4, were acquired from Acros-Organic. Nanocolor test kits of phosphate (REF 91877) from Macherey-Nagel was purchased to analyze the concentration of phosphate after adsorption.

2.2. Synthesis of sodium silicate solution

Initially, about 100 g RH was washed with tap water to eliminate foreign particles. The dried RH was dried in the oven at 60 °C for 12 h. Then, RH was burnt in the furnace at 650 °C for about 6 h to get RHA (~30 g) (Suyanta and Kuncaka, 2011). Sieved RHA was pre-treated with acid, 0.1 M HCl to remove the impurities. Extraction of sodium silicate was done by mixing 1 M NaOH solution with the RHA using a mechanical stirrer at 80 °C. After 2 h, the mixture was filtered, and the filtrate obtained was sodium silicate solution.

2.3. Synthesis of porous silica (RSi)

In this study, the adsorbent was synthesized as described in our previous work using cationic surfactant and RH-sodium silicate (Suzaimi et al., 2019). Distilled water was used to dissolved surfactant and stirred until the appearance of clear solution. Thereafter, sodium silicate derived from RH was well-mixed with surfactant solution. The pH solution of mixture was adjusted to pH 11 by dropwise addition of 1 M H_2SO_4. After stirring for 1 h, the obtained mixture was poured into Teflon autoclave and aged for 36 h at 110 °C. The solid product was filtered off, rinsed with distilled water and dried at 90 °C. The silica nanoparticles produced was denoted as RSi after 6 h calcination at 660 °C.

2.4. Functionalization and protonation of RSi-bPEI

Here, we make use of our recently used functionalization method proposed by Park et al. (2012). Schematic depiction (Fig. 1) showing the synthesis route. About 20 g of RSi was weighed and then, transferred into 200 mL glutaric dialdehyde solution and stirred homogeneously about 30 min. After that, 10% (w/v) bPEI/methanol was added to the mixture immediately and was agitated. The conditions were 30 °C for 24 h and agitation speed at 160 rpm, allowing the grafting to occurred at exterior surface and at the pore's opening. Product was filtered and thoroughly washed with distilled water. Final powdered product with 13.7 g was obtained after drying (60 °C for 24 h) was labelled as RSi-bPEI.

2.5. Preparation of protonated RSi-bPEI

Prior to adsorption testing, RSi-bPEI was acidified to convert amino groups of bPEI into ammonium salts that carry positive charge to enhance active sites of RSi-bPEI. Following the procedure reported by Hamoudi and Belkacemi (2013), 0.1 g of RSi-bPEI was agitated in 100 mL of mild HCl (0.1 M) for 6 h at room temperature as for protonation to take place. Then, protonated RSi-bPEI was washed to neutralize pH, dried and used for sorption studies.

2.6. Characterization analysis

The determination of functional group accounted for the interaction between phosphate and adsorbent was done using FTIR. For that purpose, the functional groups content of RSi- bPEI and RSi-bPEI after phosphate adsorption were determined by Fourier transform infrared (FTIR) analyzer. The elemental composition (%), i.e. carbon (C), hydrogen (H), nitrogen (N) and sulfur (S), were analyzed using Perkin Elmer CHNS analyzer. Throughout this study, transmission electron microscope (TEM) was also employed using Hitachi HT7700 TEM to examine the structural changes in terms of size and shape to examine the structure of the adsorbents before and after undergoing modification. Besides, the measurements of the porosity and Brunauer–Emmett–Teller (BET) surface area were analyzed through N_2 adsorption–desorption isotherms. Zeta potential analyzer (Zetasizer, Malvern Instruments Ltd) was used to characterize the behavior of RSi and RSi-bPEI surface. To determine the concentration of phosphate ions, phosphate test kit reagents (R.1 and R.2) were mixed with filtrate before and after adsorption and then analyzed by vis spectrometer (Macherey-Nagel).

2.7. Phosphate adsorption experiments

Performance of RSi-bPEI and RSi for phosphate adsorption was evaluated in batch equilibration mode at room tempera-

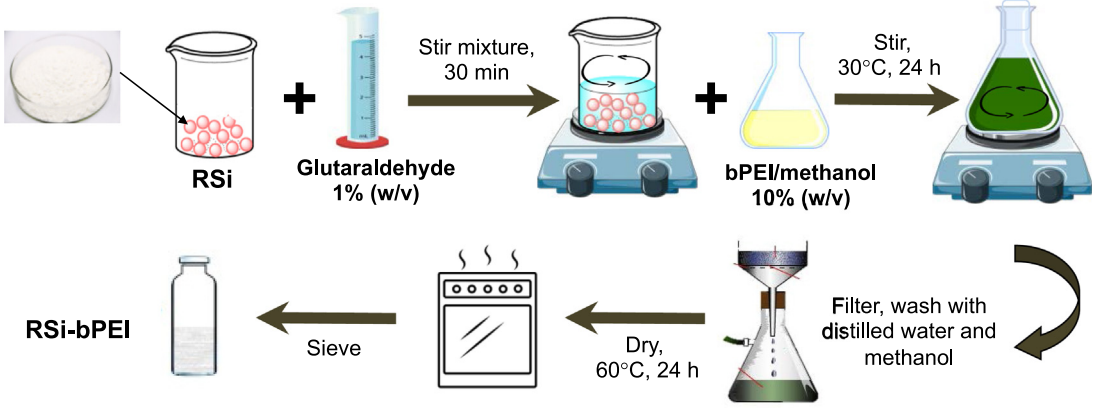

Fig. 1 Schematic representation of RSi-bPEI preparation.

ture. Unmodified RSi as a control is necessary to compare the differences on adsorption behaviors. The batch adsorption experiments were conducted by mixing a desired amount of adsorbent in 40 mL of phosphate solution in sample tube, then placed in an orbital shaker and shaken under constant shaking (170 rpm) at room temperature. Adsorption studies were performed under changing conditions of solution pH, adsorbent dosage, initial phosphate concentration and contact time, accordingly.

Effect of solution pH: Adsorption studies on the pH effect was conducted by adjusting the initial pH solution i.e. 2, 4, 5, 6, 8, 10, and 12 by micro-addition of HCl (0.1 M) or NaOH (0.1 M) solution. About 0.02 g adsorbent was added into 40 mL of 50 mg L^{-1} phosphate solution. The batch was shaken for 3 h at 170 rpm at 25 °C. The pH solution with good adsorption capacity was then further used for the next parameter test.

Effect of dose: This effect was carried out by utilizing 0.01 g, 0.02 g, 0.03 g, 0.04 g and 0.05 g of adsorbents in 40 mL of 50 mg L^{-1} nitrate and phosphate solution. The optimized pH obtained from previous section was used whereas other adsorption conditions were kept constant as abovementioned.

Effect of phosphate initial concentration: The performances was analyzed by adding 0.5 g L^{-1} adsorbent in optimal pH of solutions with initial concentration ranging from 5 to 200 mg L^{-1}. Adsorption was proceeded by shaking the batch for 3 h at 25 °C. Initial ion concentration effect is the characteristic parameter where the final equilibrium values were fixed to isotherm models.

Effect of contact time: The effect of contact time on adsorption process was determined using the optimum pH, dosage, initial concentration while contact time was adjusted in the range of 5–720 min. The results obtained were used to fit the kinetic models.

The adsorption behavior of phosphate in the presence of common competing anions in water (Cl^-, SO_4^{2-}, and HCO_3^-) were studied using initial concentration of 50 mg L^{-1} for phosphate and 30 mg L^{-1} for competing ions. All experiments were repeated for three independent batches. The adsorbed amount of phosphate per unit gram of adsorbent, q_e (mg g^{-1}) and the removal efficiency, E% were calculated by the following Eqs. (1) and (2), respectively.

$$q_e = \frac{(C_0 - C_e)v}{m} \tag{1}$$

$$E\% = \frac{(C_0 - C_e)}{C_0} \times 100\% \tag{2}$$

where q_e is equilibrium adsorption capacity (mg g^{-1}), C_0 is initial concentration of phosphate before adsorption (mg L^{-1}), C_e represents concentration after adsorption (mg L^{-1}), v is the aqueous solution volume (L), and m is amount of adsorbent (g).

2.8. Adsorption isotherms and kinetics

Adsorption isotherm experiment was conducted by allowing adsorbents to adsorb varying concentrations of phosphate solution at optimal condition. The residual phosphate concentration of the sample was analyzed after 3 h. Plot of C_e/q_e against C_e was used to calculate the Langmuir constant parameters. Meanwhile for Freundlich the values were determined from the plot ln q_e versus ln C_e Non-linear expressions of Langmuir and Freundlich were given as Eqs. (3) and (4), respectively.

$$q_e = \frac{q_m K_L C_e}{1 + K_L C_e} \tag{3}$$

$$q_e = K_F C_e^{1/n} \tag{4}$$

where q_m is maximum adsorption capacity, K_L is equilibrium constant related to binding sites (L mg^{-1}). Linear plot of Langmuir model allows the determination of q_m from the slope and K_L from the intercept of straight-line equation. K_F is Freundlich constant related to binding sites (mg g^{-1}) (L mg^{-1}) and 1/n is dimensionless heterogeneity factor. The intercept and slope of Freundlich linear plot could determine K_F and heterogeneity factor, respectively.

Dubinin-Radushkevich (D-R) model, another isotherm with high degree of regularity, was also used to fit the data. As reported, the porous structure of the adsorbent is related to the characteristic curve of D-R isotherm (Kim and Kim, 2020). It is an empirical expression model that describes adsorption mechanism with Gaussian energy distribution onto heterogeneous surfaces (Hamoudi and Belkacemi, 2013) hence, the expression is as follows (Eqs. (5) and (6)):

$$q_e = q_m \times e^{-\beta\varepsilon^2} \tag{5}$$

$$\varepsilon = RT\ln\left(1 + \frac{1}{C_e}\right) \tag{6}$$

Value of q_m and β were computed from the slope and intercept of a linear regression between ε^2 and ln C_e where β is the D-R model constant (mol^2 kJ^{-2}) giving an idea of adsorption energy and ε is the adsorption potential for the calculation of mean energy of adsorption, E (kJ mol^{-1}) per adsorbate molecules using following relationship (Eq. (7)). The R and T indicate the gas constant (8.314 J mol^{-1} K^{-1}) and absolute temperature in K, respectively.

$$E = \frac{1}{\sqrt{2\beta}} \tag{7}$$

As for kinetic study, non-linear kinetic equations for Lagergren's pseudo-first order and Ho's pseudo-second-rate laws order were used to determine the validity and kinetic mechanism of phosphate adsorption using non-linear equations Eqs. (8) and (9), respectively. In the kinetic experiments, the experiments were conducted at certain time intervals. Additionally, classical diffusion model (Weber Morris) was used to further verify the plausible diffusion mechanism and the equation is expressed as Eq. (10).

$$q_t = q_e(1 - e^{-k_1 t}) \tag{8}$$

$$q_t = \frac{k_2 q_e^2 t}{1 + k_2 q_e t} \tag{9}$$

$$q_t = \frac{k_2 q_e^2 t}{1 + k_2 q_e t} \tag{10}$$

where q_t is the amount of adsorbed phosphate at the designated time (mg g^{-1}), k_1 is the rate constant of pseudo-first-

order model (min^{-1}) and k_2 (g mg^{-1} min^{-1}) is the rate constant of pseudo-second order model, k_{id} is the intra-particle diffusion rate constant and C denotes the intercept which identified boundary layer thickness.

2.9. Desorption and reusability study

The sorbed phosphate ions could be recovered by using several stripping solutions including NaOH solution. Spent RSi-bPEI was immersed into 0.1 M of NaOH for an hour to allow phosphate ion to be released (Sowmya and Meenakshi, 2014). Then, the adsorbent was acidified with mild HCl solution to regain the adsorbents. Five cycles of adsorption–desorption were conducted batch-wise under the equilibrium conditions. Desorption efficiency was calculated from the following formula:

$$\text{Desorption efficiency } (\%) = \frac{\text{Phosphate ions desorbed}}{\text{Phosphate ions adsorbed}} \times 100\% \quad (11)$$

3. Results and discussion

3.1. Physicochemical characterizations

3.1.1. Morphological and elemental analysis

As discussed in our previous work (Suzaimi et al., 2019), RSi was observed to be spherical in shape, which similar to that of mesoporous silica MCM-41 (Jang et al., 2009; Salam et al., 2020; Thakur et al., 2017). Upon bPEI modification, although the shape was well retained, the presence of bPEI at the surroundings of the RSi was evidenced. As FESEM information is limited, the morphological properties of the as-synthesized adsorbents were further supported by TEM in this study. As synthesized RH-porous silica observed from TEM images (presented in Fig. 2) were in good agreement with the FESEM. The morphological image of RSi showed the uniform mesopores arranged into a hexagonal (honeycomb-like) lattice that resembling those of MCM-41. On the other hand, TEM image of RSi-bPEI supports the existence of bPEI on raw RSi as no clear pores can be observed Fig. 2(b). These characterization results are parallel to the low angle XRD patterns reported in our previous study where the appearance of diffraction peaks of (1 0 0), (1 1 0) and (2 0 0) indicate that RSi is silica with well ordered, forming a hexagonal lattice of MCM-41 (Suzaimi et al., 2019). Meanwhile decreased in peak intensity of the RSi-bPEI (peak 1 0 0) confirmed adsorbent pores were occupied with bPEI and hence decreased the crystallinity of RSi (Suzaimi et al., 2019).

The insets represent the weight percentage of C, H, N, and S % composition. The weight percent of N increased from 0.05% for RSi to 5.6% for RSi-bPEI confirming the presence of amino groups. These results indicated that bPEI was successfully grafted onto the adsorbent to offer more adsorption site.

3.1.2. Surface area and pore analysis

Fig. 2(c) and (d) shows N_2 adsorption–desorption isotherms of RSi and RSi-bPEI. As defined by IUPAC, above isotherms behave like type IV curves with well-defined hysteresis loop.

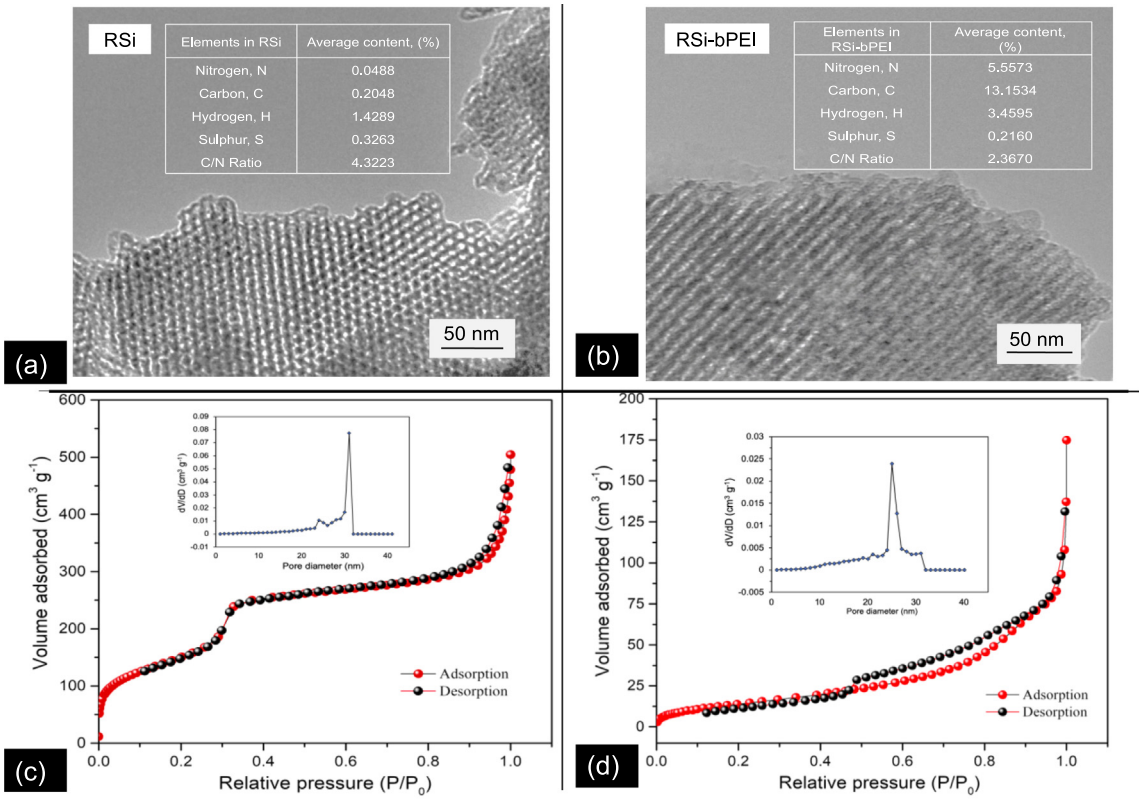

Fig. 2 Characterization of adsorbent; Elemental and morphological analysis of RSi (a) and RSi-bPEI (b); N_2 adsorption–desorption isotherms and BJH pore size distribution plot (inset) of RSi (c) and RSi-bPEI (d).

This characteristic exhibits the porous structure of the pore within the mesopore range (Jang et al., 2009). The total pore volume of RSi is 0.4919 $cm^3\ g^{-1}$ and the BET specific surface area is 546.69 $m^2\ g^{-1}$, which is in accordance to the typical RH derived porous silica (Wang et al., 2016). As can be seen in Fig. 2(d), after modification, RSi-bPEI exhibited lower N_2 adsorption. The Barrett-Joyner-Halenda (BJH) pore size distribution of the modified adsorbent was much narrower compared to the unmodified implying the mesoporous structure was altered due to the presence of bPEI. The corresponding pore sizes and specific surface area of for RSi-bPEI were reduce significantly, from 14.33 to 6.067 nm and 546.69 to 55.20 $m^2\ g^{-1}$, respectively which explained the penetration of bPEI into the porous structure of RSi-bPEI (Thakur et al., 2017) and formation of pores because of the intra- and inter-crosslinking reaction in RSi-bPEI. Modification of adsorbent suppressed the specific surface area of RSi-bPEI but increased the adsorption capacity of phosphate ions more than that RSi. The results were in line with previous work (Kim et al., 2015), which revealed that high adsorption was not necessarily rendered by the large specific surface area. The presence of specific adsorption sites arose from the desired functional groups on adsorbent as well as the porous network could also play significant roles in enhancing the efficiency of the adsorbents (Suzaimi et al., 2019).

3.1.3. Surface charge analysis

Zeta potential analysis is significant in this study to estimate and compare the surface charge of adsorbent before and after modification. The pH-zeta potential of RSi and RSi-bPEI could be found in Fig. 3. With the increasing pH values, the zeta potential value become more negative, indicating that the adsorbent surface charge was dependent on solution pH. The point of zero charge, pHpzc of RSi was found to be at 5.4, meanwhile for RSi-bPEI is around 8.9. This showed that bPEI functionalization process had increased the adsorbent surface charges from negative to positive in the entire pH ranged from 5.4 to 8.9, due to the protonated of amino groups which provided the basis for phosphate sorption by electrostatic forces. Over a wide range of pH up to pH_{pzc}, both adsorbents demonstrated a net positive zeta potential while above the pH_{pzc}, RSi and RSi-bPEI were characterized by negative surface charge due to the presence of OH^- ions.

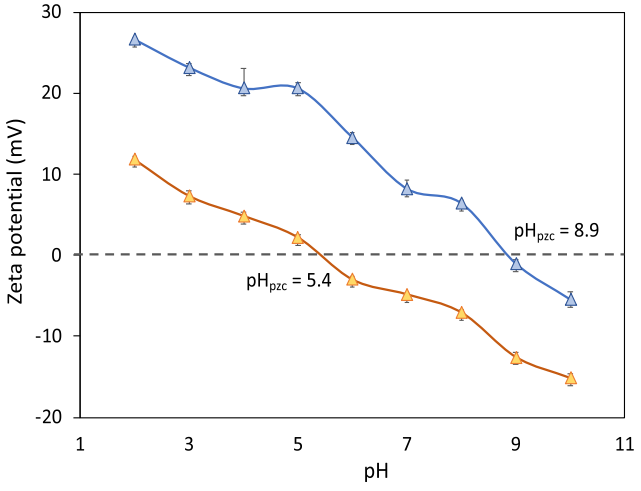

Fig. 3 Plots of zeta potential versus pH of RSi and RSi-bPEI.

3.2. Phosphate adsorption performance on various parameters

3.2.1. Solution pH

The initial pH of aqueous solution acts as an important variable in controlling adsorption capacity because this factor could significant alter the the surface charge and behavior of functional groups on the surface of adsorbent (Sani et al., 2017). Interestingly, the presence of aqueous phosphate species depends on pH variation i.e. H_3PO_4 (pH < 2), $H_2PO_4^-$ (pH 2–8), HPO_4^{2-}, (pH 8–11), and PO_4^{3-} (pH > 11), respectively (Abukhadra and Mostafa, 2019; Mng'ong'o and Sleutel, 2017) as presented in Fig. 4. Therefore, it was pertinent to study this effect for phosphate adsorption. Adsorption favored the aqueous with $H_2PO_4^-$ since the reaction of phosphate and H^+ ions predominantly involved the species compared to others (Abukhadra and Mostafa, 2019; Vikrant et al., 2018). The presence of neutral H_3PO_4 species might hinder the sorption and could be the main reason for low phosphate uptake at pH 2. However, the adsorption capacity remained high at pH 8 due to polyprotic nature of phosphate, HPO_4^{2-} (Banu and Meenakshi, 2017; Zhang et al., 2014).

The plots of adsorption capacity with respect to initial pH in Fig. 5(a) present a good adsorption result. For both RSi and RSi-bPEI, high adsorption capacity can be observed in wide pH range from 2 to 8 but high level of alkalinity (pH 10, 12) led to gradual decline in adsorption capacity. More specifically, the effect of pH relates to the surface charge where at pH < pHpzc of RSi-bPEI the surface underwent protonation in the range of 2–8.9. Protonation of active sites increased the positive charge on the surface thus the adsorption capacity was enhanced due to strong electrostatic interaction. In contrast, the adsorption capacity decreased at basic pH medium as the adsorption was restricted by the competitive interactions between the anions and the hydroxyl groups (Bhatnagar and Sillanpää, 2011).

RSi-bPEI exhibited higher adsorption capacity and removal efficiency as compared to the RSi, with the highest adsorption of 68 mg g^{-1} at the optimized pH 4 ± 0.5. This

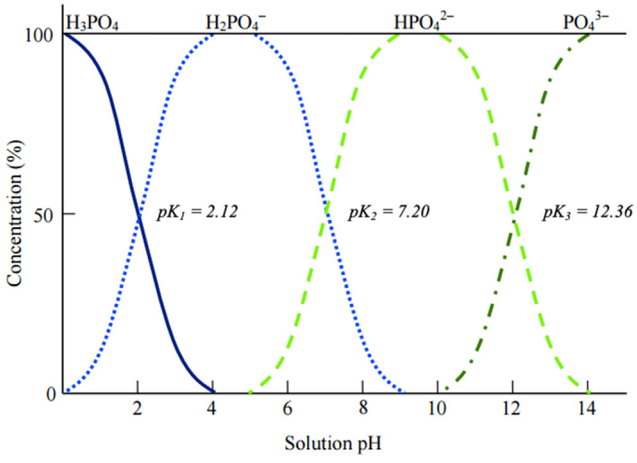

Fig. 4 Curve showing the phosphate species under varied pH values (Mng'ong'o and Sleutel, 2017).

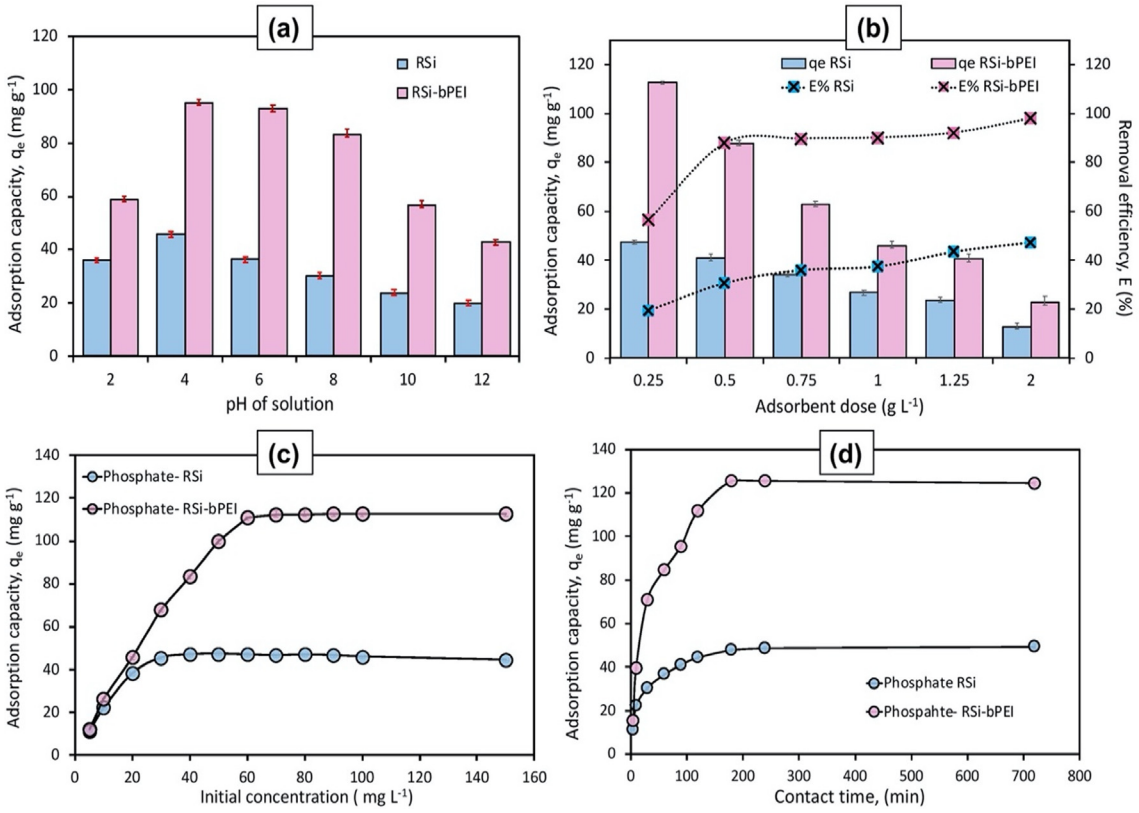

Fig. 5 Adsorption capacity of phosphate over RSi and RSi-bPEI at various parameters: (a) pH (dosage = 0.25 g L^{-1}, t = 3 h, C_0 = 50 mg L^{-1}); (b) Adsorbent dosage (pH = 4 ± 0.5, C_0 = 50 mg L^{-1}, t = 3 h); (c) Initial concentration (pH = 4 ± 0.5, dosage = 0.5 g L^{-1}, t = 3 h); (d) Time intervals (pH = 5, dosage = 0.5 g L^{-1}, C_0 = 60 mg L^{-1}).

showed that the positive surface charge of amine in RSi-bPEI facilitated the interaction through electrostatic attraction, thus enhancing adsorption capacity of RSi-PEI. However, at pH 2, adsorbents exhibited the lowest capacity. This is because H_3PO_4 presents as predominant species that weakly attached to the adsorption sites through Lewis acid-base interaction. Adsorption favored the aqueous with $H_2PO_4^-$ since the reaction of phosphate and H^+ predominantly involved $H_2PO_4^-$ compared to other species (Aswin Kumar and Viswanathan, 2018) and hence rapid adsorption occurred around pH 4–8 (Banu and Meenakshi, 2017). The species interacted with positive adsorption sites mainly via electrostatic attraction and ion exchange. Minimum phosphate adsorption at pH 10 could be related to the electrostatic repulsion between phosphate and OH^- ions. As the pH increased, strong electrostatic repulsion on the adsorbent surface was more dominant, thus preventing HPO_4^{2-} from migrating close to the surface of adsorbent consequently resulted in low phosphate uptake. Overall results suggested that bPEI-modified RSi can be used in acidic to neutral conditions with stable and promising performance.

3.2.2. Adsorbent dose

Adsorption of phosphate was enhanced with the increasing adsorbent dosage as one of the parameters in adsorption process. The variation in adsorbent dosage was carried out while maintaining the optimized parameters. Fig. 5(b) shows the similar trend as has been reported previously where the adsorption capacity decrease with the increasing of dosage (Jiang et al., 2013; Wang et al., 2018). In contrast to adsorption, the removal efficiency was increased linearly. Low adsorbent dosage of 0.2 g L^{-1} resulted in low removal due to the limited specific adsorption sites that were available for adsorption to take place. At higher adsorbent dosage, abundant adsorption sites were available for sorbent-phosphate interaction and hence removal efficiency was increased.

The removal efficiency of RSi-bPEI was close to 100%, indicating almost all phosphate ions in the solution were adsorbed. The greater adsorption capacity attained with relatively low adsorbent dosage (higher phosphate adsorbed per unit mass of adsorbent) was due to higher adsorbate/adsorbent ratio. The number of ion-exchange sites on adsorbents was increased and the adsorption on the surface was saturated more rapidly. On the other hand, further increase in adsorbent dosage resulted in a decline of adsorption capacity, as the adsorption did not reach saturation (Wang et al., 2018). By considering the removal efficiency and adsorption capacity, 0.5 g L^{-1} adsorbent dosage was chosen for further examinations.

3.2.3. Initial concentration of phosphate

The variation of initial phosphate concentration with respect to adsorption capacity was investigated in order to describe the adsorption isotherm. RSi and RSi-bPEI were employed to compare their performance and data obtained were plotted as demonstrated in Fig. 5(c). The phosphate adsorption capacity increased rapidly at low phosphate concentrations followed

by slow and small constant increase at higher concentration. The difference of ions concentration on the adsorbent and in the aqueous solution act as the driving force for the adsorption to take place at the initial stage (Aksu and Gönen, 2004). Hence, both high accessibility of adsorption active sites and the strong force between adsorbent and phosphate ions resulted in high adsorption rate. The adsorption reached equilibrium after 50 mg L^{-1} at which the saturation level (plateau) took place, reflecting that no more sites are available for further adsorption. Remarkably, adsorption capacity of RSi-bPEI, which was at least three times higher than that observed on RSi, suggested that RSi-bPEI is applicable in a broad concentration range of phosphate in wastewater.

3.2.4. Contact time

The phosphate adsorption plots at different contact times (5, 10, 30, 60, 90, 120, 240 and 720 min) is shown in Fig. 5(d). Following typical adsorption trend, phosphate adsorption increases rapidly within first 60 min. As observed from the graph, the adsorption process was partitioned into three phases. The initial one (first 60 min) was due to abundant active sites on RSi-bPEI for adsorption. The intermediate phase was relatively slow as surface attachment of phosphate ions occurred through temporary hydrogen bonding and hence saturate the active sites. After 3 h lapse the equilibrium phase or steady state was attained, with ~90% removal. Beyond this point, no significant removal of adsorption was observed related to the filling of adsorbent sites by phosphate ions with the extension of reaction time (Abukhadra et al., 2019; Abukhadra and Mostafa, 2019; Shaban et al., 2018). This revealed that the presence of bPEI in adsorbents could effectively shorten the equilibrium time compared to previous studies that took a longer time (> 24 h) to achieve the equilibrium (Fan and Zhang, 2018; Luo et al., 2016; Yin et al., 2018).

3.3. Adsorption isotherms and kinetics

3.3.1. Adsorption isotherms

Further studies on isotherms and kinetics were conducted to verify the adsorption capabilities of the samples. Adsorption equilibrium q_e, measured at equilibrium concentration solution and fixed temperature provides significant information to properly understand the adsorbate-adsorbent interaction that affect the mechanism pathways and adsorption system design (Ayawei et al., 2017). The isotherms for RSi-bPEI and RSi were therefore determined in order to assess the effect of bPEI onto its adsorption capacities. Various models have been proposed and applied to explain the equilibrium characteristics of adsorption process. Two commonly used equilibrium models, Langmuir and Freundlich were employed in this study to analyze and describe the adsorption data with an addition of D–R model that is more general than Langmuir-type isotherm. The D-R model is based on adsorption energies and ignored the influence of solution pH (Hu and Zhang, 2019; Sun et al., 2011). The corresponding plots of isotherm against the equilibrium data are shown in Fig. 6 meanwhile Table 1 summarizes the corresponding parameters. Those isotherm models differ in the basic assumption and nature of adsorbent surface.

Langmuir isotherm gives the idea about actives sites undergoing adsorption with best theoretical basis advocates that adsorption occurs at specific sites within an adsorbent until the formation of a monolayer (Langmuir, 1918). A dimensionless separation factor or equilibrium parameter, R_L, (Eq. (12)) is used to determine the feasibility of the adsorption on adsorbent. From the data, the factor R_L calculated was within the range of 0–1, corresponding to the favorability of phosphate adsorption and the bonding between anions and adsorbent

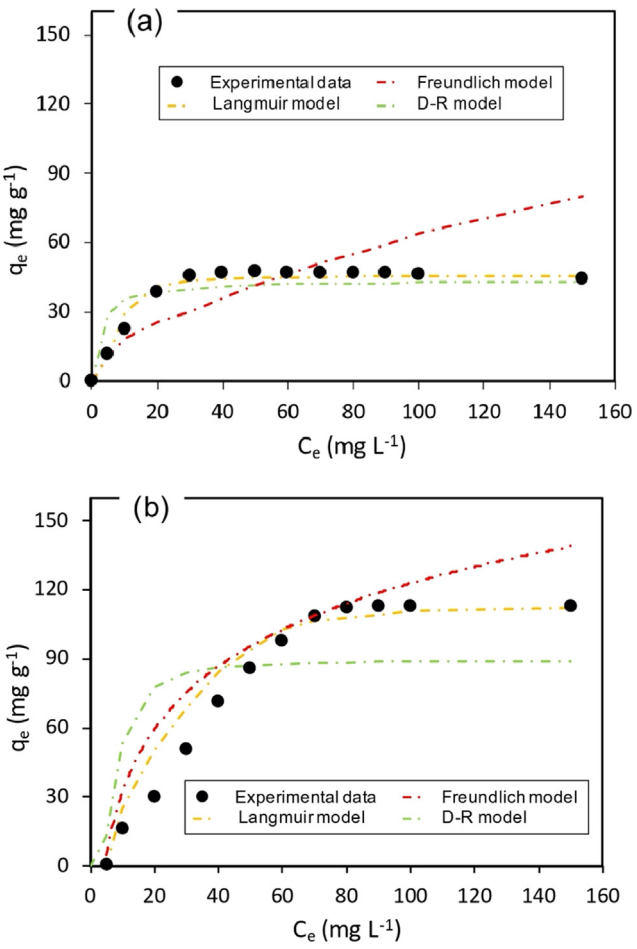

Fig. 6 Isotherm plots for phosphate adsorption on (a) RSi and (b) RSi-bPEI (pH = 4 ± 0.5; dosage = 0.5 g L^{-1}; t = 3 h).

Table 1 Isotherm parameters of phosphate adsorption on RSi and RSi-bPEI.

Isotherm model	Parameter	RSi	RSi-bPEI
Langmuir	$q_{m,\ cal}$ (mg g^{-1})	44.05	123.46
	K_L (L mg^{-1})	0.316	0.094
	R^2	0.988	0.990
	R_L	0.149	0.334
Freundlich	K_F (mg g^{-1}) (L $mg^{-1})^{1/n}$	3.680	7.248
	R^2	0.855	0.932
	n	1.677	1.625
Dubinin–Raduchkevich (D–R)	$q_{D\text{-}R\ max}$ (mg g^{-1})	45.54	89.27
	E (kJ mol^{-1})	0.326	0.235
	R^2	0.942	0.8971

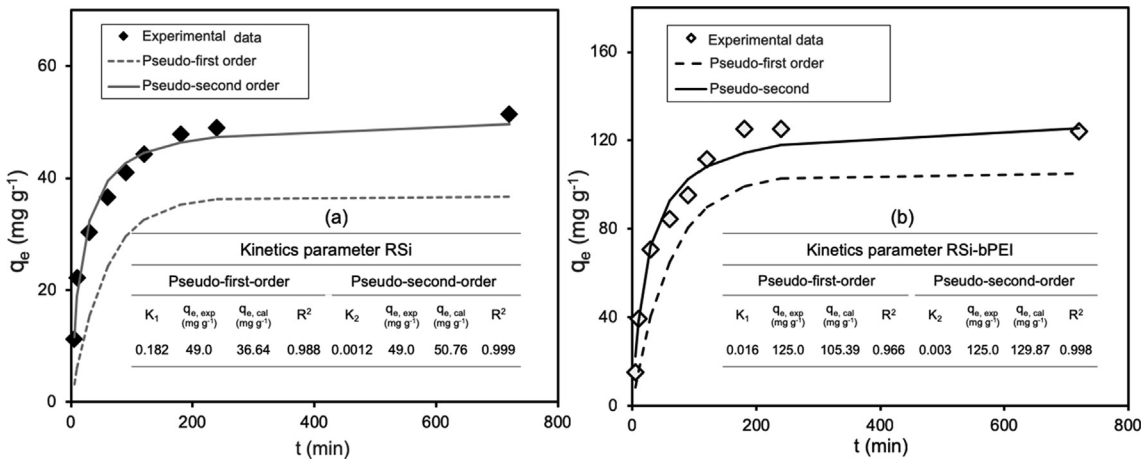

Fig. 7 Kinetics plots for phosphate adsorption on RSi (a) and RSi-bPEI (b).

surface is strong. On the other hand, Freundlich isotherm assumes that multilayer adsorption takes place on uneven surface (heterogeneous) due to the rough an irregular surface structure of adsorbent (Freundlich, 1906). The adsorption intensity of adsorbate to adsorbent in Freundlich isotherm model is referred as $1/n$. Data revealed the value of n for both adsorbents lied in between 0 and 10, suggesting adsorption process was favorable (Liu et al., 2018a).

$$R_L = \frac{1}{1 + K_L C_0} \tag{12}$$

Adsorption isotherm studies indicated that both adsorbents satisfy Langmuir, Freundlich and D-R models; the best fitted adsorption isotherm models fall in order of Langmuir > D–R > Freundlich (RSi) and Langmuir > Freundlich > D–R (RSi-bPEI). Referring to Fig. 6, the larger R^2 values (closer to 0.99) suggested that experimental adsorption isotherms were robustly fitted by the Langmuir equation for both RSi-bPEI and RSi. This implied that adsorption occurred at specific sites within an adsorbent and no other sorption can takes place at the occupied sites (Mor et al., 2017). Apart from that, this also indicated high affinity of adsorbents to the target ion pollutants (Abukhadra and Mostafa, 2019). The efficiencies of phosphate removal using different adsorbents evaluated by taking into account information on maximum adsorption capacity (q_m) and linear correlation coefficient (R^2). The higher R^2 and q_m verified the compatibility of phosphate data with Langmuir isotherm. The q_m amount of RSi-bPEI was 123.46 mg g^{-1} that is 60% higher than that of RSi, indicating the capability of RSi-bPEI to capture the phosphate ions.

D-R isotherm model is a reasonable model for the phosphate adsorption. From its expression, the magnitude of E is useful for estimating adsorption type (Ayawei et al., 2017). As tabulated in table, E values (< 8 kJ mol^{-1}) for both cases suggesting adsorption of phosphate by RSi and RSi-bPEI

Table 2 Intraparticle diffusion parameter of RSi and RSi-bPEI.

Parameter	RSi	RSi-bPEI
k_{id1} (mg g^{-1} $min^{-0.5}$)	9.83	7.424
C	11.087	11.942
R^2	0.9535	0.9792
k_{id2} (mg g^{-1} $min^{-0.5}$)	8.393	7.240
C	18.184	28.52
R^2	0.9752	0.9795
k_{id3} (mg g^{-1} $min^{-0.5}$)	0.5351	0.55
C	112.9	79.02
R^2	0.2976	0.8458

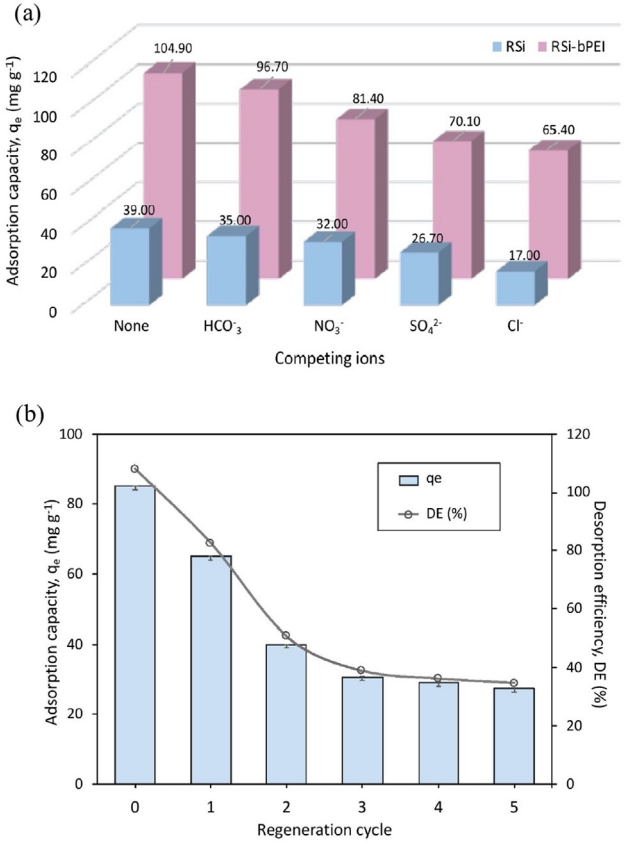

Fig. 8 (a) Influence of competing ions on phosphate adsorption over RSi-bPEI and RSi; (b) Reusability of RSi-bPEI for the phosphate adsorption (pH = 4 ± 0.5, C_0 = 50 mg L^{-1}, dosage = 0.5 g L^{-1}).

continues physically as an spontaneous process (Kong et al., 2016). It is applicable for porous adsorbent (microporous) and presumes interaction may be the results of Van der Waal's forces. This supports the fact that sorption of phosphate onto adsorbents (especially RSi) may occur through pore filling mechanism. Freundlich isotherm appeared to show low regression value as it somehow fails at higher concentration of adsorbate.

3.3.2. *Adsorption kinetics*

Thorough study to understand the adsorption mechanism was done on the adsorption reaction rate using kinetic models. The data were accessed by determining the concentration of phosphate ions at various time intervals and replotted using non-linear kinetic equations (Eqs. (8) and (9)) in order to determine the kinetic parameters (Fig. 7). Tabulated data shows consistent relation with plots, where the R^2 of the pseudo-second-order kinetic RSi and RSi-bPEI (0.99) were closer to unity than that of pseudo-first order kinetic.

The theoretical value of $q_{e,cal}$ of the pseudo-second-order kinetics were almost near to the experimental ($q_{e,exp}$). This hence prevails phosphate adsorption process obeyed pseudo-second-order kinetics. Previous studies reported that phosphate adsorption preferentially follows pseudo-second order rather than pseudo-first order (Huang et al., 2015; Liu et al., 2018b; Mazarji et al., 2017; Yin et al., 2018). The model represents the controlling rate step in this process is chemisorption where the mechanism of phosphate adsorption onto adsorbent might be promoted through either sharing or exchange of electrons between ions and adsorbents (Ebrahimi-Gatkash et al., 2015). The constant values of pseudo- second order, k_2 for RSi was smaller than RSi-bPEI, implying that a slow adsorption process is more efficient.

Since the whole adsorption process may be controlled by either one or combination of more than one step, thus the

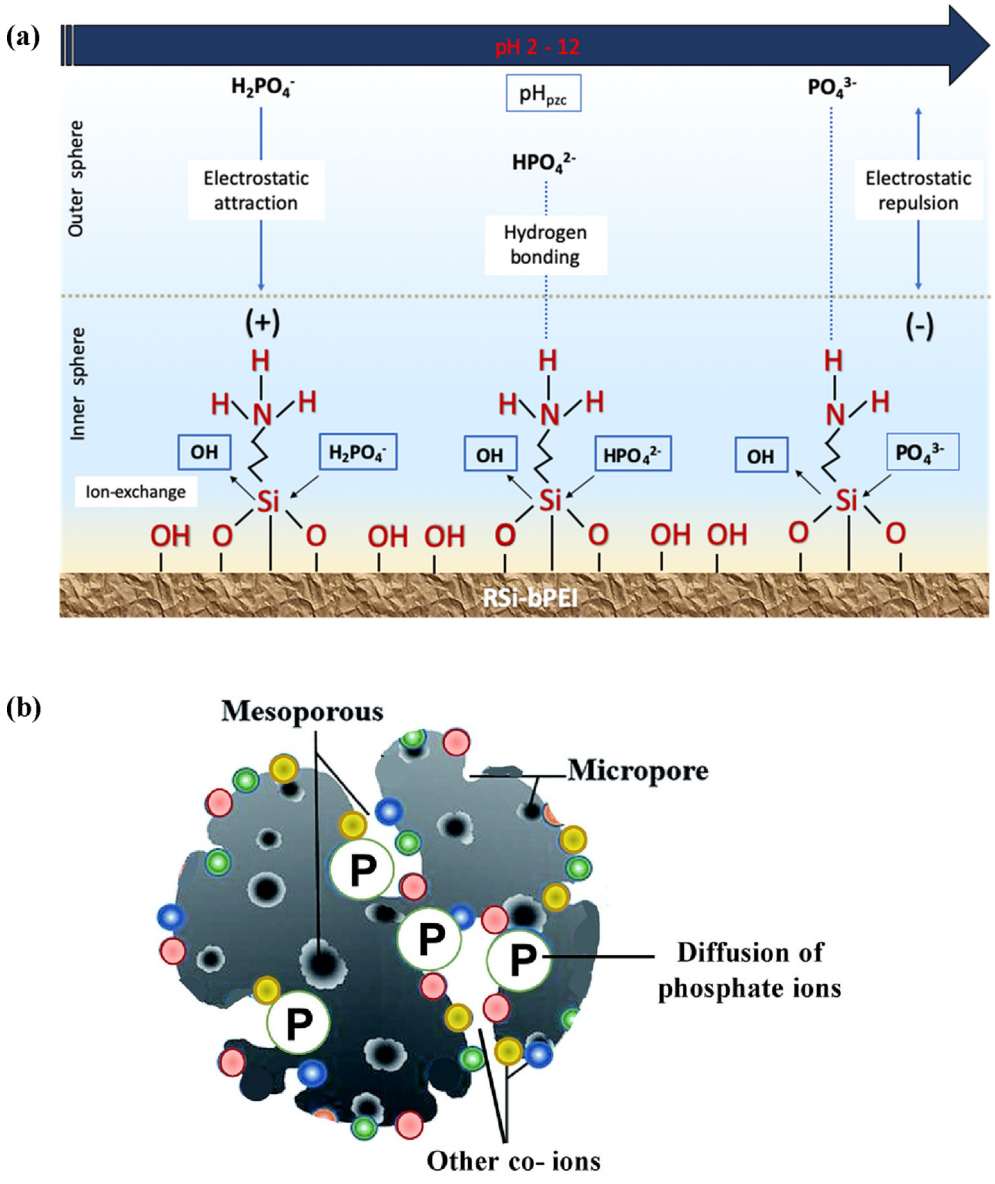

Fig. 9 Scheme showing (a) possible adsorption mechanism of phosphate ions onto RSi-bPEI in aqueous solution and (b) pore surface diffusion mechanism of phosphate onto RSi-bPEI in aqueous solution.

kinetic data were elucidated by model proposed by Weber and Morris (intraparticle diffusion) to identify the rate-determining step. This model describes several stages mechanism of fluid–solid surface as can be seen in the Table 2 i.e. external diffusion (first), intraparticle or pore diffusion (second) and adsorption on the pore surface (third). Since the data points exhibit multi-linear plots ($C \neq 0$), hence the sorption process is not intraparticle diffusion controlled and more than one sorption rates were involved during the adsorption (Fierro et al., 2008).

3.4. Sorption selectivity

The assessment of sorption selectivity was done by addition of other anions e.g. SO_4^{2-}, NO_3^-, Cl^- and HCO_3^- on phosphate solution and its removal efficiency was determined. The effect of competing ions is related to: (1) binding affinity of those ions for the adsorption sites, (2) adsorption sites competition and (3) adsorption mechanisms involved. The results showed that RSi-bPEI had a very good selectivity to phosphate in the presence of multiple ions (Fig. 8a) which indicates that these ions marginally effected phosphate adsorption capacity and removal efficiency. Nevertheless, among all ions, the presence of higher charge density ions, SO_4^{2-} imparted most inhibitory effect on phosphate adsorption, which reduced about half of corresponding values from 105 to 65.4 mg g^{-1}. In contrast to that, adsorption showed least effect on the presence of Cl^- and HCO_3^- ions. Similar trend was observed for the percentage removal and the effect of competing ions in order of $SO_4^{2-} > NO_3^- > Cl^- > HCO_3^-$.

The slight changes in adsorption performances indicated that the effect of HCO_3^- could be neglected. This could be explained by the fact that NO_3^-, Cl^- and HCO_3^- were adsorbed by forming only outer-sphere complex at the adsorbent surface. On the other hand, SO_4^{2-} and PO_4^{3-} could form either outer-sphere complex or inner-sphere which cause SO_4^{2-} to compete well with PO_4^{3-} than other competing ions. Additionally, it was also related to the stronger affinity of SO_4^{2-} towards positively adsorbent regardless of two negatively charged compared to other ions. This result is in line with the previous findings (Luo et al., 2016; Sowmya and Meenakshi, 2014).

3.5. Regeneration behavior of RSi-bPEI

For water treatment applications, prospect candidate of adsorbent must be able to be recycled, as it represents cost-effectiveness of the entire process (Sowmya and Meenakshi, 2014). Desorption study was done by elution process where the loaded adsorbents were soaked and washed using 0.1 M of NaOH and water, respectively. RSi-bPEI was then dried and reused for the phosphate adsorption. During desorption process, phosphate ions adsorbed on RSi-bPEI was replaced by OH^- of NaOH solution and the initial form of adsorbent regained after being treated with the distilled water. The interaction between phosphate and stripping solution (NaOH) is shown below:

$$Si - NH_3^+ - - - - H_2PO_4^- \xrightarrow[+NaOH]{\text{Desorption}} Si - NH_3^+ - - - - OH^-$$

$$\times \xrightarrow[+water]{} Si - NH_3^+ + H_2PO_4^-$$

The recyclability of adsorption/desorption of phosphate sorption is illustrated in Fig. 8b. Adsorption capacity towards phosphate ions reduced from 85.07 mg g^{-1} to 27.33 mg^{-1}, possibly due to the leaching of bPEI from the RSi surface. However, considerable adsorption efficiency was still observed for the subsequent cycles.

4. Proposed adsorption mechanism

The possible adsorption mechanisms of RSi-bPEI and phosphate was proposed based on the results obtained and illustrated in Fig. 9a. The mechanisms are mainly influenced by the surface functional groups of the adsorbents. This this study, phosphate species captured by the matrix of RSi-bPEI is known as inner-sphere complexation (specific adsorption), meanwhile the non-specific adsorption which is outer- sphere complexation occurred on the organic portion of the adsorbent, bPEI (Nur, 2014). The improvement of functional groups especially NH_3^+ provided more adsorption sites for phosphate ions, by forming electrostatic attraction, hydrogen bonding and ion-exchange, thereby contributing to the higher adsorption ability (Banu and Meenakshi, 2017). Also, phosphate ions moved into the pores of RSi-bPEI by diffusion mechanism (Fig. 9b).

As evidenced from the characterization results, the point of zero charge, pH_{pzc} of RSi-bPEI was 8.9, so within the range of pH 2.0–8.0, RSi-bPEI was protonated and positively charged. The dominant species available in low to medium pH solution were $H_2PO_4^-$ and HPO_4^{2-} ions and thus, phosphate ions non-specifically captured to the RSi-bPEI surface through electrostatic attraction (between positively charged adsorbents with the negatively charge of phosphate species). The interaction between the phosphate anions and the protonated RSi- bPEI surface can be expressed as:

$$Si - NH_3^+ + H_2PO_4^- \rightarrow Si - NH_3^+ - - - - H_2PO_4^-$$

Besides electrostatic attraction, phosphate ions could possibly form inner sphere complexes with the active sites of RSi-bPEI. It happened when OH^- from the adsorbent being replaced by phosphate species e.g. $H_2PO_4^-$. FT-IR spectra of RSi and RSi-bPEI before and after adsorption were presented in Fig. 10. The appearance peaks of phosphate at ~1100 cm^{-1}

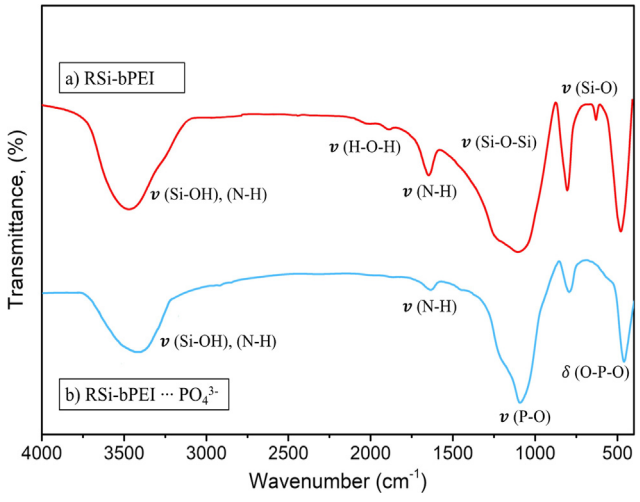

Fig. 10 FTIR spectra of RSi-bPEI after phosphate adsorption.

Table 3 List of phosphate adsorption performance by various adsorbents.

No	Adsorbents	Contact time (min)	pH of solution	q_m (mg g^{-1})	Reusability (cycles)	Reference
1	RSi–bPEI	180	4.5	123.46	5	This study
2	Ti (VI) nanocomposite	240	6.5–7	44.14	5	Nie et al. (2019)
3	Al–modified biochar	1440	< 6	57.49	–	Yin et al. (2018)
4	Dipolar hydroxyethyl cellulose	45	5	46.9	–	Ray et al. (2018)
5	Amine–$CuFe_2O_4$ chelated with La	1440	5.5	32.59	–	Gu et al. (2018)
6	La doped magnetic graphene	30	6–8	116.28	5	Rashidi Nodeh et al. (2017)
7	Zr–reduced GO	1440	5	27.71	–	Luo et al. (2016)
8	RH/MCM–41	30	6	21.01	–	Seliem et al. (2016)
9	Biomass–activated carbon residue	2	6	3.48	–	Kilpimaa et al. (2014)
10	Fe_3O_4/ZrO_2/chitosan	1440	3	26.5	–	Jiang et al. (2013)

and bend vibration of O—P—O confirming the theory of phosphate ions were adsorbed onto the RSi-bPEI surface through inner-sphere complexation (Yin et al., 2018) In addition, amine stretching vibration seemed less intense after adsorption process, indicating that the active sites of RSi-bPEI had reacted with phosphate ions. The process is considered as:

$$Si–OH + H_2PO_4^- \rightarrow Si–H_2PO_4^- + OH^-$$

In acidic condition, ion exchange between phosphate ions and chloride on the matrix could also be regarded as a potential mechanism.

Other probable mechanism exhibited by phosphate ions is hydrogen bonding. Hydrogen in amine groups established with oxygen present in phosphate ions as shown below:

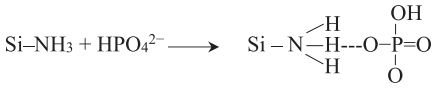

Model of intraparticle diffusion showed the occurrence of pore diffusion mechanism in this removal process. However, it is not the sole rate limiting step according to the low values of the rate constant, k_i and layer thickness, C obtained. The diffusion mechanism illustration was illustrated in Fig. 9b.

The comparison with some of other adsorbents from previous studies is summarized in Table 3. From the table, one can see that RSi-bPEI is significantly high in most cases and comparable in a few cases in terms of adsorption capacity for phosphate. High phosphate adsorption capacity achieved by RSi-bPEI might be due to the porous structure, high specific surface area and importantly the presence of large quantities of amine groups resulted from the highly branched structure PEI groups that enabled the sorption process to consistently take place. It is anticipated that this novel adsorbent can be an attractive alternative for potential used in real field application. To further extend the economic feasibility, future research is needed to improve the recyclability of the adsorbent. As temperature is an additional factor that can influence the sorption process, the effect of the temperature should be of great interest to provide more insights into the optimization of the adsorption process.

5. Conclusion

An adsorbent focusing on affordability, environmental considerations, reusable and promising properties was successfully synthesized by utilizing RH producing RSi. Modification of bPEI onto RSi, with large amount of amino functional groups, provided more specific adsorption sites and accelerate the adsorption. Isotherms and kinetics studies implied that Langmuir isotherms and pseudo-second-order model were the best models to satisfactorily describe the sorption behavior of phosphate on RSi and RSi-bPEI. bPEI. Langmuir maximum adsorption capacity of RSi-bPEI reached approximately 123.46 mg g^{-1}, which outperformed that of unmodified RSi by about 60% under the best operational conditions. In adsorption study of co-ions, SO_4^{2-} significantly altered the adsorption capacity of phosphate while the effects of other anions were negligible. From the practical point of view, RSi-bPEI exhibited a good utilization efficiency since desorption-adsorption recycle inspected shows a little decrease in desorption efficiency (~70%) during 5th cycle. Reports in the literature on the phosphate adsorption capacity for RSi-bPEI is comparable with that of other adsorbents, revealing RSi-bPEI as a prospect adsorbent in environmental pollution control.

Declaration of Competing Interest

The authors declared that there is no conflict of interest.

Acknowledgement

The authors acknowledge the financial support provided by Ministry of Higher Education Malaysia under Fundamental Research Grant Scheme (FRGS) 5F005 and HiCOE grant (4J435).

References

Abukhadra, M.R., Adlii, A., Bakry, B.M., 2019. Green fabrication of bentonite/chitosan@cobalt oxide composite (BE/CH@Co) of enhanced adsorption and advanced oxidation removal of Congo red dye and Cr (VI) from water. Int. J. Biol. Macromol. 126, 402–413. https://doi.org/10.1016/j.ijbiomac.2018.12.225.

Abukhadra, M.R., Mostafa, M., 2019. Effective decontamination of phosphate and ammonium utilizing novel muscovite/phillipsite composite; equilibrium investigation and realistic application. Sci. Total Environ. 667, 101–111. https://doi.org/10.1016/j.scitotenv.2019.02.362.

Aksu, Z., Gönen, F., 2004. Biosorption of phenol by immobilized activated sludge in a continuous packed bed: prediction of

breakthrough curves. Process Biochem. 39, 599–613. https://doi.org/10.1016/S0032-9592(03)00132-8.

Alexander, D., Ellerby, R., Hernandez, A., Wu, F., Amarasiriwardena, D., 2017. Investigation of simultaneous adsorption properties of Cd, Cu, Pb and Zn by pristine rice husks using ICP-AES and LA-ICP-MS analysis. Microchem. J. 135, 129–139. https://doi.org/10.1016/j.microc.2017.08.001.

Aswin Kumar, I., Viswanathan, N., 2018. Development and reuse of amine-grafted chitosan hybrid beads in the retention of nitrate and phosphate. J. Chem. Eng. Data 63, 147–158. https://doi.org/10.1021/acs.jced.7b00751.

Ayawei, N., Ebelegi, A.N., Wankasi, D., 2017. Modelling and interpretation of adsorption isotherms. J. Chem. 2017, 3039817. https://doi.org/10.1155/2017/3039817.

Banu, H.T., Meenakshi, S., 2017. One pot synthesis of chitosan grafted quaternized resin for the removal of nitrate and phosphate from aqueous solution. Int. J. Biol. Macromol. 104, 1517–1527. https://doi.org/10.1016/j.ijbiomac.2017.03.043.

Barbosa, T.R., Foletto, E.L., Dotto, G.L., Jahn, S.L., 2018. Preparation of mesoporous geopolymer using metakaolin and rice husk ash as synthesis precursors and its use as potential adsorbent to remove organic dye from aqueous solutions. Ceram. Int. 44, 416–423. https://doi.org/10.1016/j.ceramint.2017.09.193.

Bhatnagar, A., Sillanpää, M., 2011. A review of emerging adsorbents for nitrate removal from water. Chem. Eng. J. 168, 493–504. https://doi.org/10.1016/j.cej.2011.01.103.

Choi, J.-W., Lee, S.-Y., Chung, S.-G., Hong, S.-W., Kim, D.-J., Lee, S.-H., 2011. Removal of phosphate from aqueous solution by functionalized mesoporous materials. Water Air Soil Pollut. 222, 243–254. https://doi.org/10.1007/s11270-011-0820-y.

Chowdhury, S., 2017. Rice husk is a natural low-cost adsorbent for reactive dyes. Int. Res. J. Adv. Eng. Sci. 2, 70–74.

Delaney, P., McManamon, C., Hanrahan, J.P., Copley, M.P., Holmes, J.D., Morris, M.A., 2011. Development of chemically engineered porous metal oxides for phosphate removal. J. Hazard. Mater. 185, 382–391. https://doi.org/10.1016/j.jhazmat.2010.08.128.

Dinker, M.K., Ajithkumar, T.G., Kulkarni, P.S., 2017. l-Proline functionalized dicationic framework of bifunctional mesoporous organosilica for the simultaneous removal of lead and nitrate ions. ACS Sustain. Chem. Eng. 5, 4188–4196. https://doi.org/10.1021/acssuschemeng.7b00132.

Ebrahimi-Gatkash, M., Younesi, H., Shahbazi, A., Heidari, A., 2015. Amino-functionalized mesoporous MCM-41 silica as an efficient adsorbent for water treatment: batch and fixed-bed column adsorption of the nitrate anion. Appl. Water Sci. 7, 1887–1901. https://doi.org/10.1007/s13201-015-0364-1.

Fan, C., Zhang, Y., 2018. Adsorption isotherms, kinetics and thermodynamics of nitrate and phosphate in binary systems on a novel adsorbent derived from corn stalks. J. Geochem. Explor. 188, 95–100. https://doi.org/10.1016/J.GEXPLO.2018.01.020.

Fierro, V., Torné-Fernández, V., Montané, D., Celzard, A., 2008. Adsorption of phenol onto activated carbons having different textural and surface properties. Microporous Mesoporous Mater. 111, 276–284. https://doi.org/10.1016/j.micromeso.2007.08.002.

Freundlich, H.M.F., 1906. Over the adsorption in solution. J. Phys. Chem. A 57, 385–471. https://doi.org/10.1515/zpch-1907-5723.

Gu, W., Li, X., Xing, M., Fang, W., Wu, D., 2018. Removal of phosphate from water by amine-functionalized copper ferrite chelated with La(III). Sci. Total Environ. 619–620, 42–48. https://doi.org/10.1016/j.scitotenv.2017.11.098.

Gupta, V.K., Tyagi, I., Sadegh, H., Ghoshekand, R.S., Makhlouf, A. S.H., Maazinejad, B., 2015. Nanoparticles as adsorbent; A positive approach for removal of noxious metal ions: A review. Sci. Technol. Dev. 34, 195–214. https://doi.org/10.3923/std.2015.195.214.

Hamoudi, S., Belkacemi, K., 2013. Adsorption of nitrate and phosphate ions from aqueous solutions using organically-functionalized silica materials: Kinetic modeling. Fuel 110, 107–113. https://doi.org/10.1016/j.fuel.2012.09.066.

Hamoudi, S., Saad, R., Belkacemi, K., 2007. Adsorptive removal of phosphate and nitrate anions from aqueous solutions using ammonium-functionalized mesoporous silica. Ind. Eng. Chem. Res. 46, 8806–8812. https://doi.org/10.1021/ie070195k.

He, Y., Lin, H., Dong, Y., Li, B., Wang, L., Chu, S., Luo, M., Liu, J., 2018. Zeolite supported Fe/Ni bimetallic nanoparticles for simultaneous removal of nitrate and phosphate: Synergistic effect and mechanism. Chem. Eng. J. 347, 669–681. https://doi.org/10.1016/j.cej.2018.04.088.

Hu, Q., Zhang, Z., 2019. Application of Dubinin-Radushkevich isotherm model at the solid/solution interface: A theoretical analysis. J. Mol. Liq. 277, 646–648. https://doi.org/10.1016/j.molliq.2019.01.005.

Huang, W., Yu, X., Tang, J., Zhu, Y., Zhang, Y., Li, D., 2015. Enhanced adsorption of phosphate by flower-like mesoporous silica spheres loaded with lanthanum. Microporous Mesoporous Mater. 217, 225–232. https://doi.org/10.1016/j.micromeso.2015.06.031.

Hubadillah, S.K., Othman, M.H.D., Harun, Z., Ismail, A.F., Rahman, M.A., Jaafar, J., 2017. A novel green ceramic hollow fiber membrane (CHFM) derived from rice husk ash as combined adsorbent-separator for efficient heavy metals removal. Ceram. Int. 43, 4716–4720. https://doi.org/10.1016/J.CERAMINT.2016.12.122.

Jang, H.T., Park, Y., Ko, Y.S., Lee, J.Y., Margandan, B., 2009. Highly siliceous MCM-48 from rice husk ash for CO_2 adsorption. Int. J. Greenh. Gas Control 3, 545–549. https://doi.org/10.1016/j.ijggc.2009.02.008.

Jiang, H., Chen, P., Luo, S., Tu, X., Cao, Q., Shu, M., 2013. Synthesis of novel nanocomposite Fe_3O_4/ZrO_2/chitosan and its application for removal of nitrate and phosphate. Appl. Surf. Sci. 284, 942–949. https://doi.org/10.1016/j.apsusc.2013.04.013.

Kilpimaa, S., Runtti, H., Kangas, T., Lassi, U., Kuokkanen, T., 2014. Removal of phosphate and nitrate over a modified carbon residue from biomass gasification. Chem. Eng. Res. Des. 92, 1923–1933. https://doi.org/10.1016/j.cherd.2014.03.019.

Kim, J.Y., Balathanigaimani, M.S., Moon, H., 2015. Adsorptive removal of nitrate and phosphate using MCM-48, SBA-15, chitosan, and volcanic pumice. Water. Air. Soil Pollut. 226, 1–11. https://doi.org/10.1007/s11270-015-2692-z.

Kim, M.-S., Kim, J.-G., 2020. Adsorption characteristics of spent coffee grounds as an alternative adsorbent for cadmium in solution. Environments 7, 24. https://doi.org/10.3390/environments7040024.

Kiran, B.R., Prasad, M.N.V., 2019. Biochar and rice husk ash assisted phytoremediation potentials of Ricinus communis L. for lead-spiked soils. Ecotoxicol. Environ. Saf. 183, 109574. https://doi.org/10.1016/j.ecoenv.2019.109574.

Kong, H., Cheu, S., Othman, N.S., Song, S., Saman, N., Johari, K., Mat, H., 2016. RSC Advances Surfactant modi fi cation of banana trunk as low- cost adsorbents and their high benzene adsorptive removal performance from aqueous solution. RSC Adv. 6, 24738–24751. https://doi.org/10.1039/C6RA00911E.

Langmuir, I., 1918. Adsorption of gases on plain surfaces of glass mica platinum. J. Am. Chem. Soc. 40, 1361–1403. https://doi.org/10.1006/ceps.2001.1094.

Lee, J.H., Kwon, J.H., Lee, J.W., Lee, H Sun, Chang, J.H., Sang, B.I., 2017. Preparation of high purity silica originated from rice husks by chemically removing metallic impurities. J. Ind. Eng. Chem. 50, 79–85. https://doi.org/10.1016/j.jiec.2017.01.033.

Liu, N., Wang, H., Weng, C.-H., Hwang, C.-C., 2018a. Adsorption characteristics of Direct Red 23 azo dye onto powdered tourmaline. Arab. J. Chem. 11, 1281–1291. https://doi.org/10.1016/J.ARABJC.2016.04.010.

Liu, T., Feng, J., Wan, Y., Zheng, S., Yang, L., 2018b. ZrO_2 nanoparticles confined in metal organic frameworks for highly

effective adsorption of phosphate. Chemosphere 210, 907–916. https://doi.org/10.1016/j.chemosphere.2018.07.085.

Luo, X., Wang, X., Bao, S., Liu, X., Zhang, W., Fang, T., 2016. Adsorption of phosphate in water using one-step synthesized zirconium-loaded reduced graphene oxide. Sci. Rep. 6, 1–13. https://doi.org/10.1038/srep39108.

Matori, K.A., Haslinawati, M.M., Wahab, Z.A., Sidek, H.A.A., Ban, T.K., Ghani, W.A.W.A.K., 2009. Producing amorphous white silica from rice husk. J. Basic Appl. Sci. 1, 512–515.

Mazarji, M., Aminzadeh, B., Baghdadi, M., Bhatnagar, A., 2017. Removal of nitrate from aqueous solution using modified granular activated carbon. J. Mol. Liq. 233, 139–148. https://doi.org/10.1016/j.molliq.2017.03.004.

Mng'ong'o, M., Sleutel, S. promotor (viaf)188812309, 2017. Competition between Organic Matter and Phosphate for Binding Sites in Sandy Soils.

Mor, S., Chhoden, K., Negi, P., Ravindra, K., 2017. Utilization of nano-alumina and activated charcoal for phosphate removal from wastewater. Environ. Nanotechnol. Monit. Manag. 7, 15–23. https://doi.org/10.1016/j.enmm.2016.11.006.

Moritz, M., Geszke-Moritz, M., 2019. The effect of SBA-15 surface modification on the process of 18β-glycyrrhetinic acid adsorption: modeling of experimental adsorption isotherm data. Materials (Basel) 12, 3671. https://doi.org/10.3390/ma12223671.

Nasir, A.M., Md Nordin, N.A.H., Goh, P.S., Ismail, A.F., 2018. Application of two-dimensional leaf-shaped zeolitic imidazolate framework (2D ZIF-L) as arsenite adsorbent: Kinetic, isotherm and mechanism. J. Mol. Liq. 250, 269–277. https://doi.org/10.1016/j.molliq.2017.12.005.

Nie, G., Wu, L., Du, Y., Wang, H., Xu, Y., Ding, Z., Liu, Z., 2019. Efficient removal of phosphate by a millimeter-sized nanocomposite of titanium oxides encapsulated in positively charged polymer. Chem. Eng. J. 360, 1128–1136. https://doi.org/10.1016/j.cej.2018.10.184.

Nur, T., 2014. Nitrate, phosphate and fluoride removal from water using adsorption process. University of Technology, Sydney. PhD Thesis.

Omotunde, I., Okoronkwo, A., Oluwashina, O., 2018. Derived and thiourea-functionalized silica for cadmium removal: Isotherm, kinetic and thermodynamic studies. Appl. Water Sci. 8, 1–13. https://doi.org/10.1007/s13201-018-0652-7.

Park, S.-I., Kwak, I.S., Bae, M.A., Mao, J., Won, S.W., Han, D.H., Chung, Y.S., Yun, Y.-S., 2012. Recovery of gold as a type of porous fiber by using biosorption followed by incineration. Bioresour. Technol. 104, 208–214. https://doi.org/10.1016/J.BIORTECH.2011.11.018.

Patil, R., Rajendra, D., Jyotsna, M., 2014. Preparation of silica powder from rice husk. Agric. Eng. Int. CIGR J. 19, 158–161.

Production of high purity amorphous silica from rice husk, rdquo; 2016. Procedia Chemistry 19, 189–195. https://doi.org/10.1016/j.proche.2016.03.092. Submitted for publication.

Rashidi Nodeh, H., Sereshti, H., Zamiri Afsharian, E., Nouri, N., 2017. Enhanced removal of phosphate and nitrate ions from aqueous media using nanosized lanthanum hydrous doped on magnetic graphene nanocomposite. J. Environ. Manage. 197, 265–274. https://doi.org/10.1016/j.jenvman.2017.04.004.

Ray, J., Jana, S., Tripathy, T., 2018. Macromolecules synthesis of dipolar grafted hydroxyethyl cellulose and its application for the removal of phosphate ion from aqueous medium by adsorption. Int. J. Biol. Macromol. 109, 492–506. https://doi.org/10.1016/j.ijbiomac.2017.12.083.

Salam, M.A., AbuKhadra, M.R., Mohamed, A.S., 2020. Effective oxidation of methyl parathion pesticide in water over recycled glass based-MCM-41 decorated by green Co3O4 nanoparticles. Environ. Pollut. 259, 113874. https://doi.org/10.1016/j.envpol.2019.113874.

Sani, H.A., Ahmad, M.B., Hussein, M.Z., Ibrahim, N.A., Musa, A., Saleh, T.A., 2017. Nanocomposite of ZnO with montmorillonite for removal of lead and copper ions from aqueous solutions. Process Saf. Environ. Prot. 109, 97–105. https://doi.org/10.1016/J.PSEP.2017.03.024.

Sanz, R., Calleja, G., Arencibia, A., Sanz-Pérez, E.S., 2010. CO_2 adsorption on branched polyethyleneimine-impregnated mesoporous silica SBA-15. Appl. Surf. Sci. 256, 5323–5328. https://doi.org/10.1016/j.apsusc.2009.12.070.

Seliem, M.K., Komarneni, S., Abu Khadra, M.R., 2016. Phosphate removal from solution by composite of MCM-41 silica with rice husk: Kinetic and equilibrium studies. Microporous Mesoporous Mater. 224, 51–57. https://doi.org/10.1016/j.micromeso.2015.11.011.

Shaban, M., Abukhadra, M.R., Khan, A.A.P., Jibali, B.M., 2018. Removal of Congo red, methylene blue and Cr(VI) ions from water using natural serpentine. J. Taiwan Inst. Chem. Eng. 82, 102–116. https://doi.org/10.1016/j.jtice.2017.10.023.

Sowmya, A., Meenakshi, S., 2014. Effective removal of nitrate and phosphate anions from aqueous solutions using functionalised chitosan beads. Desalin. Water Treat. 52, 2583–2593. https://doi.org/10.1080/19443994.2013.798842.

Sun, X.F., Wang, S.G., Cheng, W., Fan, M., Tian, B.H., Gao, B.Y., Li, X.M., 2011. Enhancement of acidic dye biosorption capacity on poly(ethylenimine) grafted anaerobic granular sludge. J. Hazard. Mater. 189, 27–33. https://doi.org/10.1016/j.jhazmat.2011.01.028.

Suyanta, Kuncaka, A., 2011. Utilization of rice husk as raw material in synthesis of mesoporous silicates MCM-41. Indones. J. Chem. 11, 279–284.

Suzaimi, N.D., Goh, P.S., Malek, N.A.N.N., Lim, J.W., Ismail, A.F., 2019. Performance of branched polyethyleneimine grafted porous rice husk silica in treating nitrate-rich wastewater via adsorption. J. Environ. Chem. Eng. 7, 103235. https://doi.org/10.1016/j.jece.2019.103235.

Thakur, A.K., Nisola, G.M., Limjuco, L.A., Parohinog, K.J., Torrejos, R.E.C., Shahi, V.K., Chung, W.J., 2017. Polyethylenimine-modified mesoporous silica adsorbent for simultaneous removal of Cd(II) and Ni(II) from aqueous solution. J. Ind. Eng. Chem. 49, 133–144. https://doi.org/10.1016/j.jiec.2017.01.019.

Vikrant, K., Kim, K.H., Ok, Y.S., Tsang, D.C.W., Tsang, Y.F., Giri, B.S., Singh, R.S., 2018. Engineered/designer biochar for the removal of phosphate in water and wastewater. Sci. Total Environ. 616–617, 1242–1260. https://doi.org/10.1016/j.scitotenv.2017.10.193.

Wang, J., Liu, Y., Hu, P., Huang, R., 2018. Adsorption of phosphate from aqueous solution by Zr(IV)-crosslinked quaternized chitosan /bentonite composite. Environ. Prog. Sustain. Energy 37, 267–275. https://doi.org/10.1002/ep.12667.

Wang, X.X., Wu, Y.H., Zhang, T.Y., Xu, X.Q., Dao, G.H., Hu, H.Y., 2016. Simultaneous nitrogen, phosphorous, and hardness removal from reverse osmosis concentrate by microalgae cultivation. Water Res. 94, 215–224. https://doi.org/10.1016/j.watres.2016.02.062.

Yaumi, A.L., Bakar, M.Z.A., Hameed, B.H., 2018. Melamine-nitrogenated mesoporous activated carbon derived from rice husk for carbon dioxide adsorption in fixed-bed. Energy 155, 46–55. https://doi.org/10.1016/j.energy.2018.04.183.

Yin, Q., Ren, H., Wang, R., Zhao, Z., 2018. Evaluation of nitrate and phosphate adsorption on Al-modified biochar: influence of Al content. Sci. Total Environ. 631–632, 895–903. https://doi.org/10.1016/j.scitotenv.2018.03.091.

Zhang, L., Gao, Y., Zhou, Q., Kan, J., Wang, Y., 2014. High-performance removal of phosphate from water by graphene nanosheets supported lanthanum hydroxide nanoparticles. Water. Air. Soil Pollut. 225, 1967–1978. https://doi.org/10.1007/s11270-014-1967-0.

Zulfiqar, U., Subhani, T., Wilayat Husain, S., 2015. Towards tunable size of silica particles from rice husk. J. Non. Cryst. Solids 429, 61–69. https://doi.org/10.1016/j.jnoncrysol.2015.08.037.